Title: Identification of scavenger receptor B1 as the airway microfold cell receptor for *Mycobacterium tuberculosis*

Authors: Haaris S. Khan[1], Vidhya R. Nair[1], Cody R. Ruhl[1], Samuel Alvarez-Arguedas[1], Jorge L. Galvan Resendiz[1], Luis H. Franco[1]*, Linzhang Huang[2], Philip W. Shaul[2], Ron B. Mitchell[3] and Michael U. Shiloh[1,4]**.

Affiliations:

[1]Department of Internal Medicine, University of Texas Southwestern Medical Center, Dallas, TX.

[2]Center for Pulmonary and Vascular Biology, Department of Pediatrics, University of Texas Southwestern Medical Center, Dallas, TX.

[3]Department of Otolaryngology, University of Texas Southwestern Medical Center, Dallas, TX.

[4]Department of Microbiology, University of Texas Southwestern Medical Center, Dallas, TX.

*Present address: Luis H. Franco, Federal University of Minas Gerais, Belo Horizonte, Minas Gerais, Brazil

**Correspondence to: Michael.Shiloh@UTSouthwestern.edu

Abstract: *Mycobacterium tuberculosis* (Mtb) can enter the body through multiple routes, including via specialized transcytotic cells called microfold cells (M cell). However, the mechanistic basis for M cell entry remains undefined. Here, we show that M cell transcytosis depends on the Mtb Type VII secretion machine and its major virulence factor EsxA. We identify scavenger receptor B1 (SR-B1) as an EsxA receptor on airway M cells. SR-B1 is required for Mtb binding to and translocation across M cells in mouse and human tissue. Together, our data demonstrate a previously undescribed role for Mtb EsxA in mucosal invasion and identify SR-B1 as the airway M cell receptor for Mtb.

Running title: SR-B1 is an airway M cell receptor for Mtb EsxA

Introduction

Mycobacterium tuberculosis (Mtb), the causative agent of tuberculosis (TB), latently infects roughly one-third of the world's population and causes 1-2 million deaths per year. The current paradigm of acute infection is that after an actively infected person aerosolizes infectious Mtb-containing particles, a naïve individual inhales the bacteria that then traverse the respiratory tree to ultimately be phagocytosed by alveolar macrophages (Churchyard et al., 2017; Cohen et al., 2018). While this model can account for pulmonary TB, it is insufficient to explain some extrapulmonary forms of TB initiated by oropharyngeal infection and lacking evidence of concurrent pulmonary disease. For example, a disease known as tuberculous cervical lymphadenopathy, or scrofula, represents 10% of all new cases of TB, and frequently manifests without lung involvement (Fontanilla et al., 2011). Because the oropharynx and upper airway lymphatics drain to the cervical lymph nodes, while the lower airway lymphatics drain to the mediastinal lymph nodes, infection of the cervical lymph nodes by Mtb may not involve the lower airways. Indeed, in the infamous "Lübeck Disaster" where hundreds of infants and children were accidentally orally administered Mtb instead of the attenuated BCG vaccine, the majority developed lymphatic and oropharyngeal TB rather than pulmonary TB (Fox et al., 2016), highlighting how inoculation via the oropharyngeal route can cause extrapulmonary disease.

One potential explanation for the development of lymphatic TB centers upon the mucosa-associated lymphoid tissue (MALT) (Brandtzaeg et al., 2008). Specialized epithelial cells known as M cells overlie the MALT and are able to translocate luminal material to basolateral antigen presenting cells located immediately beneath the M cell (Kimura, 2018). In this way, M cells can

initiate an immune response to pathogens or material found within the lumen (Nakamura et al., 2018).

Since their initial discovery overlying Peyer's patches of the gastrointestinal tract, M cells have been identified at other mucosal sites. Within the respiratory tract, M cells have been found in the upper and lower airways of both mice and humans (Fujimura, 2000; Kim et al., 2011; Kimura et al., 2019). M cells express a number of pattern recognition receptors (PRRs) (Mabbott et al., 2013). The majority of these M cell receptors have been identified on gastrointestinal M cells, while receptor expression by airway microfold cells is less will understood. Some PRRs on gastrointestinal M cells function in bacterial recognition and translocation. For example, the cellular prion protein (PrP(C)), a receptor for *Brucella abortus*, is necessary for *B. abortus* translocation (Nakato et al., 2012). Similarly, glycoprotein 2 (GP2) expressed on the apical surface of gastrointestinal M cells recognizes FimH, a component of the type I pili found on both commensal and pathogenic bacteria (Hase et al., 2009). Loss of either the host receptor GP2 or the bacterial ligand FimH diminishes bacterial translocation through M cells, reducing the immune response to these antigens and bacteria within Peyer's patches (Hase et al., 2009).

We previously demonstrated that Mtb uses airway M cells as a portal of entry to initiate infection (Nair et al., 2016). We hypothesized that Mtb may produce a bacterial effector to mediate this process, and that, similar to receptors for Gram-negative bacteria in the gastrointestinal tract (Hase et al., 2009), airway M cells may also encode an Mtb receptor. Here we show that Mtb requires the type VII secretion system for translocation in vitro and in vivo. The type VII secretion system effector EsxA is sufficient to mediate this process in vitro through binding to scavenger receptor class B type I (SR-B1). SR-B1 is enriched on mouse and human M cells both in vitro and in vivo. Loss of SR-B1 reduces EsxA and Mtb binding to M cells, and prevents Mtb translocation

through M cells in vitro. Using a newly developed explanted human adenoid model, we demonstrate robust expression of SR-B1 on primary human M cells. Finally, we show that Mtb infects primary human M cells on adenoids in a type VII secretion system dependent manner. Taken together, our findings indicate that the interaction of Mtb EsxA with M cell SR-B1 allows Mtb to traverse the airway mucosa to initiate infection.

Results

The Mtb type VII secretion system mediates Mtb binding to and translocation through M cells in vitro

Mtb encodes several protein secretion systems important for bacterial virulence (Feltcher et al., 2010). One of the type VII secretion systems (T7SS) of Mtb, contained within the region of difference 1 (RD1) locus of Mtb (Behr et al., 1999), secretes virulence factors including EsxA and EsxB (CFP-10) (Stanley et al., 2003) (Fig. 1A). We hypothesized that the Mtb T7SS might facilitate M cell translocation because the T7SS machine interacts directly with eukaryotic membranes (Augenstreich et al., 2017), EsxA can be identified on the mycobacterial cell surface (Kinhikar et al., 2010), and EsxA may directly bind several cell surface receptors (Kinhikar et al., 2010; Sreejit et al., 2014). To test if the Mtb T7SS was required for bacterial binding to and translocation across M cells, we used a human airway M cell transwell model we developed previously (Nair et al., 2016). Such transwells combine 16-HBE cells (Cozens et al., 1994) in the apical compartment of a transwell and Raji B cells in the basolateral compartment in order to mimic the organization of MALT and to enhance M cell formation (Kerneis et al., 1997; Nair et al., 2016). HBE cells cultured alone form a homogenous, polarized monolayer (hereafter called "control") while coculture with Raji B cells induces some HBE cells to differentiate into M cells

(hereafter called "HBE/Raji B") (Nair et al., 2016). We used the Mtb*ΔeccD1* strain, which lacks the inner membrane pore required for assembly of and protein secretion by the T7SS (Fig. 1A) (Abdallah et al., 2007). To test if the Mtb T7SS was necessary for M cell binding, we incubated transwells with either mCherry expressing wild-type Mtb (WT Mtb) or mCherry expressing Mtb*ΔeccD1* at 4°C to prevent bacterial entry or translocation and analyzed surface binding by confocal microscopy and quantification of colony-forming units (CFU) (Fig. 1B-D). Consistent with our prior data (Nair et al., 2016), significantly more WT Mtb bound HBE/Raji B transwells (containing M cells) than control transwells by both microscopy (Fig. 1B,C) and CFU (Fig. 1D). However, binding was greatly reduced for the Mtb*ΔeccD1* strain (Fig. 1B-D).

To test if the Mtb T7SS is necessary to facilitate mycobacterial translocation across M cells, we infected the apical chamber of transwells with either WT Mtb or Mtb*ΔeccD1* and measured translocation to the basal compartment. As we reported previously(Nair et al., 2016), WT Mtb translocated across HBE/Raji B transwells to a greater extent than control transwells, while the translocation of the Mtb*ΔeccD1* strain was significantly reduced (Fig. 1E). Importantly, the transepithelial electrical resistance (TEER), a measure of epithelial monolayer integrity (Srinivasan et al., 2015), was stable during the experiment (Fig. 1F). To further verify that Mtb T7SS is required for bacterial translocation across M cells in vitro, we also utilized an established model of M cell differentiation where Caco-2 cells, a human colonic epithelial cell line, are cultured with Raji B transwells to induce M cell differentiation (Nair et al., 2016). Similar to HBE/Raji B transwells, we observed that Mtb translocated across Caco-2/Raji B transwells in a T7SS dependent manner (Fig. 1G). Taken together, these data show that the Mtb T7SS is necessary for both binding to and translocation across M cells in vitro.

EsxA is sufficient to mediate binding to and translocation across M cells in vitro

Two of the most abundant T7SS secreted proteins are EsxA and EsxB; therefore, we hypothesized that one of these proteins might mediate Mtb binding and translocation. We conjugated recombinant EsxA, EsxB, or glycine (as a control) to fluorescent beads, added the beads to the apical chamber of transwells, and quantified bead translocation to the basal compartment by flow cytometry. EsxA-beads but not control beads translocated across HBE/Raji B transwells (Fig. 2A) without disrupting the epithelial monolayer (Fig. 2B). EsxA-beads, but not EsxB-beads or control beads, also translocated across Caco-2/Raji B transwells (Fig. 2C).

To test if the ability of EsxA to mediate translocation was due to direct EsxA binding to M cells, we incubated transwells with recombinant EsxA and performed immunofluorescence microscopy using antibodies against EsxA and α1,2-fucose (NKM 16-2-4; a marker for M cells (Nair et al., 2016; Nochi et al., 2007)) (Fig. 2D). While both groups of transwells had equal number of nuclei per field (Fig. 2E), HBE/Raji B transwells had more NKM 16-2-4 positive M cells compared to control transwells (Fig. 2F). We detected robust EsxA binding to M cells on HBE/Raji B transwells (Fig. 2D,G-H). Similar results were observed using an antibody against Sialyl Lewis^A (SLA), a different M cell marker (Giannasca et al., 1999; Nair et al., 2016) (Supp. Fig. 1). Taken together, these data demonstrate that EsxA directly binds the M cell surface and is sufficient to mediate translocation across M cells when conjugated to inert beads.

Scavenger receptor class B type 1 binds EsxA and is expressed on M cells in vitro

Because EsxA bound directly to the surface of M cells, we hypothesized that EsxA may engage a cell surface receptor. To affinity purify cell surface binding proteins we performed a modified co-immunoprecipitation experiment using either EsxA or transferrin crosslinked to the TriCEPS reagent, a molecule that allows for the covalent cross-linking of a ligand and its receptor

(Tremblay and Hill, 2017). We used Caco-2 cells for this experiment as they have been used extensively as a model for M cells in vitro (Tyrer et al., 2006) and because Caco-2/Raji B transwells behaved similarly to HBE/Raji B transwells in Mtb and EsxA translocation (Fig. 1E,G and Fig. 2A,C). Using this approach, we identified the interaction between transferrin (TRFE) and the transferrin receptor (TFR1) (Fig. 3A, blue peptides), proving the validity of this system. When cells were treated with EsxA, peptides for two proteins, apolipoprotein E (ApoE) and scavenger receptor class B type I (SR-B1) were enriched (Fig. 3A, red peptides). Because ApoE is a soluble protein (Huang and Mahley, 2014) while SR-B1 is a known cell surface molecule, we focused on SR-B1. For further verification, we performed a co-immunoprecipitation/biotin transfer experiment without the TriCEPS reagent. After incubation with biotinylated EsxA, completion of the biotin transfer assay, and subsequent immunoprecipitation with streptavidin-coated beads, western blotting with an anti-SR-B1 antibody detected a 130 kD band likely reflecting a heavily glycosylated SR-B1 isoform (Zanoni et al., 2016), along with a fainter band at approximately 55 kD consistent with the non-glycosylated SR-B1 protein (Fig. 3B).

We next determined if SR-B1 expression is specific for M cells or ubiquitously expressed by epithelial cells. We quantified colocalization of SR-B1 and NKM 16-2-4 by immunofluorescence microscopy in control and HBE/Raji B transwells (Fig. 3C-F). While there was no difference in the number of nuclei per field on the transwells (Fig. 3C), SR-B1 expression was higher on HBE/Raji B transwells (Fig. 3C,E) and the majority of the SR-B1 positive cells were M cells (Fig. 3C,F). Taken together, we identify SR-B1 as a candidate EsxA receptor expressed on M cells in vitro.

Genetic disruption of SR-B1 limits EsxA binding to M cells

We next investigated whether SR-B1 is required for EsxA binding to M cells. We transduced HBE cells with non-targeting (NT) or *SR-B1* shRNA and observed a robust knock-down of SR-B1 in HBE cells transduced with the *SR-B1* shRNA as compared to the NT shRNA (Fig. 4A). HBE/Raji B transwells constructed from these cells had a similar number of M cells comparing NT and *SR-B1* shRNA transwells (Fig. 4B,C) and *SR-B1* shRNA transwells showed a reduction in SR-B1 expression by immunofluorescence microscopy (Fig. 4B,D). Loss of SR-B1 reduced the number of EsxA positive cells on HBE/Raji B *SR-B1* shRNA transwells (Fig. 4B,E). Additionally in HBE/RajiB NT shRNA transwells, the majority of EsxA positive cells were SR-B1 positive (Fig. 4B,F), suggesting that EsxA preferentially bound SR-B1 expressing M cells. Taken together, we identify SR-B1 as necessary for EsxA binding to M cells.

Genetic disruption of SR-B1 reduces both Mtb binding to and translocation across M cells

To determine the role of SR-B1 in Mtb binding to M cells, we incubated HBE/Raji B transwells expressing NT or *SR-B1* shRNAs with mCherry Mtb at 4°C for 1 hr and analyzed binding by confocal microscopy and CFU (Fig. 4G-I). Loss of SR-B1 greatly reduced the number of bacteria bound to the HBE/Raji B transwells as determined by confocal microscopy (Fig. 4G,H) and by quantification of CFU (Fig. 4I). To determine the role of SR-B1 in Mtb translocation by M cells, we infected HBE/Raji B transwells expressing NT or *SR-B1* shRNAs with Mtb in the apical compartment and measured translocation to the basal compartment. As expected from the reduced bacterial binding (Fig. 4G-I), loss of SR-B1 also greatly reduced Mtb translocation in the HBE/Raji B transwells at 37°C (Fig. 4J) with no impact on the TEER (Fig. 4K). The reduced ability of Mtb to translocate across HBE/Raji B transwells expressing *SR-B1* shRNA was not due to any intrinsic defect in translocation caused by SR-B1 deficiency as another airway pathogen, *Pseudomonas aeruginosa*, was able to translocate equally across NT and *SR-B1* shRNA HBE/Raji B transwells

(Fig. 4L). Of note, *P. aeruginosa* does not encode a T7SS or EsxA homologue, suggesting that its translocation across M cells depends on unique bacterial and host factors. We thus conclude that SR-B1 is essential for the binding and translocation of Mtb via M cells in a process requiring the effector EsxA.

The Mtb type VII secretion system is necessary for Mtb translocation in mice

M cells are found in the upper and lower airways of mice and humans (Fujimura, 2000; Mutoh et al., 2016; Nair et al., 2016; Teitelbaum et al., 1999). We therefore determined if SR-B1 was expressed preferentially by primary M cells as compared to other epithelial cells using immunofluorescence microscopy. Mouse nasal-associated lymphoid tissue (NALT), a region enriched for M cells (Mutoh et al., 2016; Nair et al., 2016; Park et al., 2003), demonstrated robust SR-B1 staining on the surface of NKM 16-2-4 positive cells (Fig. 5A). Importantly, we did not observe SR-B1^{+}/NKM 16-2-4^{-} cells, demonstrating that SR-B1 is specific for M cells in the NALT epithelia in vivo.

We and others previously demonstrated that NALT and airway M cells are a portal of entry for Mtb in mice (Nair et al., 2016; Teitelbaum et al., 1999). To determine if the Mtb T7SS is necessary for bacterial translocation in vivo, we performed NALT infections (Nair et al., 2016) with MtbΔ*eccD1* or MtbΔ*esxA*. In both Mtb mutant strains the T7SS machine fails to assemble (Abdallah et al., 2007) thereby preventing T7SS-dependent virulence factor secretion. We infected mice intranasally with WT Mtb, MtbΔ*eccD1* (Fig. 5B), or MtbΔ*esxA* (Fig. 5C) and enumerated CFU from draining cervical lymph nodes 7 days post-infection (Nair et al., 2016). Both the MtbΔ*eccD1* and MtbΔ*esxA* strains had 1.0-1.5 log fewer bacteria compared to WT Mtb in the cervical lymph nodes. This degree of attenuation was not observed when we infected mice

intranasally with a Cor deficient strain of Mtb (Mtb*cor::Tn7)* that is also attenuated in vivo (Zacharia et al., 2013) (Supp. Fig. 2). Taken together, these data demonstrate that the lower CFU recovered from cervical lymph nodes of mice infected with T7SS mutant Mtb strains may be due to reduced translocation across M cells.

Human adenoid M cells express SR-B1

Because TB is a human disease, we tested if primary human M cells can serve as a portal of entry for Mtb. The human adenoid is a MALT structure that contains M cells interspersed among the overlying epithelial cells (Fujimura, 2000). We first demonstrated that human adenoids contain SR-B1 positive M cells by immunofluorescence microscopy (Fig. 5D), similar to our observations from mouse NALT. We confirmed the presence of M cells in human adenoids by flow cytometry (Supp. Fig. 3 for gating strategy) and observed that approximately 10% of the adenoid cells were $EpCAM^{+}/NKM^{-}$ epithelial cells, while about 1% of the cells were $EpCAM^{+}/NKM^{+}$ double positive M cells (Fig. 5E). When we analyzed SR-B1 expression using flow cytometry, we observed that approximately 20% of primary human M cells (marked as $EpCAM^{+}/NKM^{+}$ cells) were SR-B1 positive as compared to less than 2% of the other epithelial cells ($EpCAM+/NKM^{-}$) (Fig. 5F), verifying our observation that SR-B1 is expressed predominately by M cells in vivo.

Human adenoid M cells are a portal of entry for Mtb

To determine if primary human M cells can be a route of entry for Mtb, we infected human adenoids with GFP+ Mtb and quantified the number of GFP^{+} Mtb $EpCAM^{+}/NKM^{+}$ M cells versus GFP^{+} Mtb $EpCAM^{+}/NKM^{-}$ epithelial cells by flow cytometry (Fig. 5G, Supp. Fig. 4 for gating strategy). The number of GFP^{+} Mtb containing $EpCAM^{+}/NKM^{+}$ M cells cells ranged from 0.1-8% while we were unable to identify any GFP^{+} Mtb containing $EpCAM^{+}/NKM^{-}$ epithelial cells,

suggesting that M cells were a preferred route of entry for Mtb in adenoids. Finally, we determined the role of the Mtb T7SS in Mtb entry into adenoid M cells. We infected adenoids with GFP^+ WT Mtb or GFP^+ MtbΔ*eccD1* and observed more GFP^+/$EpCAM^+$/NKM^+ cells after infection with WT Mtb as compared to MtbΔ*eccD1* (Fig. 5H). Taken together, we conclude that Mtb can enter via mouse NALT and human adenoid M cells in a T7SS dependent manner.

Discussion

In this work, we used in vitro and in vivo M cell models to demonstrate a mucosal interaction between Mtb EsxA and the cell surface protein SR-B1. EsxA, a protein secreted through the T7SS, bound M cells in vitro, was sufficient to mediate M cell translocation by inert beads and was necessary for Mtb translocation in vitro. Furthermore, the T7SS was necessary for Mtb translocation in a mouse mucosal infection model. Primary human airway M cells internalized Mtb in a T7SS dependent manner, indicating that this process is relevant for human disease. Finally, SR-B1 was enriched on M cells and served as a receptor for Mtb EsxA to mediate Mtb translocation. Together, our data demonstrate a previously undescribed role for Mtb EsxA in mucosal invasion and identify SR-B1 as the airway M cell receptor for Mtb.

EsxA has previously been implicated as a secreted pore-forming molecule (Smith et al., 2008), though this activity has recently been questioned (Conrad et al., 2017). In our experiments utilizing recombinant EsxA we also did not observe pore formation or epithelial damage. This could be due to the relatively short amount of time we incubated EsxA with our transwells for binding or translocation experiments. Alternatively, the pore forming properties of EsxA may only occur when the protein is in low pH conditions, such as in the lysosome. Thus, EsxA may directly interact with M cell SR-B1 in a cell contact dependent manner (Conrad et al., 2017), leading to SR-B1 receptor mediated internalization similar to its function in both hepatitis C virus and

Plasmodium vivax uptake (Heo et al., 2006; Manzoni et al., 2017). Though SR-B1 has not been previously identified as an EsxA receptor, prior studies have found other host proteins that interact with EsxA, including laminin (Kinhikar et al., 2010), β2 microglobulin (Sreejit et al., 2014), and TLR-2 (Pathak et al., 2007). We did not identify these proteins in our affinity purification assay, a discrepancy possibly related to the cell types used for binding experiments.

In mice, we observed that Mtb lacking the T7SS had a greatly reduced ability to disseminate from mouse NALT to the cervical lymph nodes, potentially due to a reduced ability to translocate across M cells. A possible alternate interpretation for this result centers on the observation that T7SS deficient strains of Mtb are attenuated in vivo and in macrophages (Stanley et al., 2003). Thus, the reduced CFU recovered from draining lymph nodes could represent a macrophage survival defect for the T7SS deficient strains. However, when we used a different attenuated Mtb strain for NALT infection, we observed normal dissemination to the draining lymph nodes. We therefore propose that the reduced CFU recovered from cervical lymph nodes of mice infected with T7SS-deficient Mtb is not simply due to an attenuation defect within macrophages. Consistent with this interpretation, the markedly reduced translocation of T7SS-deficient Mtb across M cells in vitro and into explanted human adenoids ex vivo, in the absence of an innate immune response and over a very short time course, indicates that the T7SS is required for translocation across M cells.

SR-B1 has been well characterized as a high-density lipoprotein receptor involved in cholesterol uptake (Shen et al., 2018). It has also been shown that SR-B1 binds several bacterial molecules, including lipopolysacharide and lipoteicheic acid produced by Gram-negative and Gram-positive bacteria respectively (Bocharov et al., 2004). Although direct interaction of EsxA and SR-B1 has not previously been shown, SR-B1 has been reported as a receptor for mycobacteria

(Philips et al., 2005; Schafer et al., 2009), primarily in macrophages (Stamm et al., 2015). However, when SR-B1$^{-/-}$ mice were infected with Mtb via the aerosol route, there was no difference in bacterial replication, granuloma size, cytokine secretion, or survival within the first four months post-infection compared to wild-type mice (Schafer et al., 2009). Based on our current data and previous results showing improved mouse survival during aerosol Mtb infection when M cells are reduced (Nair et al., 2016), we predict that loss of M cell SR-B1 should reduce bacterial dissemination from the airway and enhance mouse survival. SR-B1$^{-/-}$ mice experience defective intrauterine and post-natal development and as a result are not born at normal Mendellian ratios (Santander et al., 2013). In addition, they manifest increased serum HDL, cardiovascular defects and altered adrenal hormones (Trigatti et al., 1999), making them incompatible with such a study. Likewise, mice expressing an M-cell specific Cre have not been reported, preventing analysis of SR-B1 function exclusively in M cells.

Adenoid M cells may serve as a portal of entry for Mtb, with significant implications for Mtb pathogenesis in humans. Because respiratory MALT is more abundant in children than adults (Tschernig and Pabst, 2000) and M cells are a key component of MALT (Corr et al., 2008), we propose that the increased incidence of extrapulmonary TB in children (Yang et al., 2004) is due to M cell mediated translocation. Interestingly, there was significant variation in M cell entry in human adenoids, which could relate to polymorphisms in SR-B1 or differences in SR-B1 expression by M cells. We speculate that M cell invasion may be a common phenomenon for other pathogens that invade via the airway, including *Bacillus anthracis*, *Streptococcus pneumonia* or *Streptococcus pyogenes*, and such pathogens may also utilize M cell receptors for entry.

In conclusion, we demonstrate that M cells are a portal of entry for Mtb in vitro, in mouse NALT, and in human adenoids. Utilizing mouse models and in vitro models, we identify EsxA

and SR-B1 as a molecular synapse required for Mtb translocation across M cells in vitro and in vivo in both mice and humans. A greater understanding of the role of airway M cells in the context of infection by Mtb or other respiratory pathogens will yield insight into novel pathways with potential for new vaccine candidates or therapeutics.

Materials and Methods:

Bacterial strains and Media

M. tuberculosis Erdman, *M. tuberculosis* Erdman Δ*eccD1* (Stanley et al., 2003), *M. tuberculosis* Erdman Δ*esxA* (Stanley et al., 2003), *M. tuberculosis* Erdman *cor:Tn7* (Zacharia et al., 2013) were grown in Middlebrook 7H9 medium or on Middlebrook 7H11 plates supplemented with 10% oleic acid-albumin-dextrose-catalase. Tween 80 (Fisher T164-500) was added to liquid medium to a final concentration of 0.05%.

Cell culture

The human colorectal adenocarcinoma cell line Caco-2 (HTB-37) and human Burkitt lymphoma cell line Raji B (CCL-86) were obtained from ATCC (Manassas, VA, USA). 16HBE14o- cells (Forbes et al., 2003) were provided by Dieter Gruenert (University of California, San Francisco). Caco-2 or HBE cells were grown in DMEM (Gibco 11965092) supplemented with 20% fetal bovine serum (Gibco 26140079), 50 units/mL penicillin (Gibco 15140122), 50 µg/mL streptomycin (Gibco 15140122), 2 mM L-glutamine (Gibco 25030081), 1% sodium pyruvate (Gibco 11360070), 1% non-essential amino acids (Gibco 11140050), and 1 mM HEPES (Hyclone SH30237.01). Raji B cells were grown in DMEM supplemented with 20% FBS and 2 mM L-glutamine. In order to generate stable knock-down lines of SR-B1, HBE cells were transduced with lentivirus containing the appropriate shRNA cloned into pLKO.1 (Addgene 10878) as

317 described previously (Huang et al., 2019). Transduced cells were selected with puromycin (Sigma-
318 Aldrich P8833-10MG) and surviving cells were maintained in puromycin for three additional
319 passages.

320 **Tissue bilayer model**

321 3 x 10^5 Caco-2 or HBE cells in 1 mL of media were plated in the upper chamber of a 3 μm
322 transwell insert (Corning 3462). For Raji B treated transwells, 5 x 10^5 Raji B cells in 2 mL of
323 media were added to the basal compartment, thereby inducing some of the overlying epithelial
324 cells to differentiate into M cells. For control transwells, 2 mL of media alone were added to the
325 basal chamber, leading to little to no M cell differentiation. 1 mL of media in the upper chamber
326 and 1 mL of media in the bottom chamber were aspirated daily and replaced with 1 mL of fresh
327 media. The transwells were maintained at 37°C for 2 weeks or until the transepithelial electrical
328 resistance was greater than 350Ω. 72 hours prior to infection, transwells were cultured in media
329 lacking antibiotics. Transwell media was changed approximately 2 hours prior to infection.

330 **In vitro Mtb infection**

331 Liquid cultures of Mtb were grown until mid-log phase, washed three times with PBS, and
332 centrifuged and sonicated to remove clumps. Bacteria were then resuspended in DMEM + 20%
333 fetal bovine serum. For translocation assays, bacterial inoculum was added to the upper chamber
334 of the transwell at a MOI of 5:1 and media from the basal compartment was sampled after 60
335 minutes. The samples were then plated on 7H11 agar plates and maintained in a 37°C incubator
336 for 3 weeks to allow for colony formation.

337 **Protein expression and purification**

338 gBlocks (IDT) encoding Mtb EsxA or EsxB were first cloned into the pENTR entry vector
339 (Thermo K240020) then subcloned into the pDest17 destination vector (Thermo 11803012;

Thermo 11791020) using Gateway cloning (Invitrogen) per the manufacturer's protocol. The resulting vectors were cloned into the BL21 strain of *E. coli* (NEB C2527I) for protein expression. 1 L of bacterial culture was grown to an OD600 of 0.6, induced with 1 mM IPTG (Promega V3955) at 37°C for 3 hours, and centrifuged at 3500 rpm for 15 minutes at 4°C to yield a bacterial pellet. The bacterial pellet was then resuspended in 15 mL of resuspension buffer (50 mM sodium phosphate, 500 mM NaCl, pH 7.4) with one tablet of EDTA-free protease inhibitor (Roche 11836170001). Bacteria were lysed by sonication and centrifuged at 11200 rpm for 15 minutes at 4°C. The resulting pellet was resuspended in 20 mL of 8 M urea in resuspension buffer and incubated for 2 hours at room temperature with gentle agitation. The protein slurry was again centrifuged at 11200 rpm for 15 minutes at 4°C and the resulting supernatant was incubated with cobalt TALON affinity resin (Clontech 635503) for 2 hours at room temperature. Resin was washed with 8 M urea in resuspension buffer and EsxA or EsxB was eluted with 150 mM imidazole and 8 M urea in resuspension buffer. The eluate was dialyzed overnight using a Slide-a-Lyzer dialysis cassette (Thermo 66203) against 10 mM ammonium bicarbonate. The dialyzed sample was again incubated with cobalt TALON affinity resin for 2 hours at room temperature. Resin was subsequently washed with 10 mM Tris-HCl pH 8.0, 0.5% ASB-14 (Sigma A1346-1G) in 10 mM Tris-HCl pH 8.0, and 10 mM Tris-HCl pH 8.0. EsxA or EsxB was eluted with 150 mM imidazole in PBS, dialyzed overnight against PBS, and stored at 4°C.

Tissue bilayer immunofluorescence microscopy

In order to image binding of Mtb to transwells, mCherry Mtb was grown until mid-log phase, washed, and centrifuged and sonicated to remove clumps. The bacterial inoculum was added to the upper chamber of the transwell at a MOI of 5:1 for 2 hours at 4°C with gentle agitation every 15 minutes. Transwells were gently washed and fixed with 4% paraformaldehyde in PBS at

4°C for one hour. Transwell inserts were stained with DAPI (Thermo D1306), excised using a blade, mounted on microscope slides using Prolong Gold antifade reagent (Invitrogen P36390) and imaged using an AxioImager MN microscope (Zeiss). In order to image binding of EsxA to transwells, EsxA was expressed and purified as described above. EsxA was then biotinylated by the Sulfo-SBED reagent (Thermo 33033) per manufacturer's instructions and excess reagent was removed using PD-10 desalting columns (GE Healthcare 17-0851-01). Transwells were then incubated with 1.5 μM EsxA in HBSS for 2 hours at 4°C with gentle agitation, washed, and exposed to UV light for 30 minutes at room temperature to allow for cross-linking. Transwells were then fixed with 4% paraformaldehyde in PBS for 15 minutes at room temperature, blocked with 10% donkey serum (Sigma D9663-10ML) in PBS for three hours at room temperature, and incubated with a 1:100 dilution of rabbit anti-SR-B1 antibody (Abcam 52629) in 2% donkey serum in PBS overnight at 4°C. The following day, transwells were washed and incubated with a 1:100 dilution of PE-conjugated rat NKM 16-2-4 (Miltenyi 130-102-150), a 1:500 dilution of an AlexaFluor 647 conjugated donkey-anti-rabbit secondary antibody (Thermo A-31573), and a 1:500 dilution of AlexaFluor 488 conjugated streptavidin (Jackson 016-540-084) for 1 hour at room temperature. Transwells were then washed, stained with DAPI, excised with a blade, mounted, and imaged as described above.

Microsphere conjugation and translocation

Microspheres were conjugated to protein as per instructions (Polylink 24350-1). Briefly, 12.5 mg of microspheres were centrifuged and washed twice in coupling buffer. Microspheres were then incubated with an EDAC/coupling buffer solution to activate the microspheres. 200 μg of protein is added to the beads, thereby allowing for covalent binding of the protein to the microspheres. Microspheres are then washed twice with PBS and stored at 4°C. In order to test the

ability of these beads to translocate in the tissue bilayer assay, beads were diluted to a MOI of 5:1 in DMEM + 20% fetal bovine serum and added to the apical chamber of transwells. Media from the basal compartment was sampled after 60 minutes and the number of beads present in the sample was analyzed by flow cytometry using an LSR II flow cytometer (BD).

TriCEPS screen

For initial conjugation of TriCEPS to protein, EsxA or transferrin (300 µg) dissolved in 150 µL 25 mM HEPES pH 8.2 buffer was added to 1.5 µL of the TriCEPS reagent (Dualsystems Biotech) and incubated at 20°C for 90 minutes with gentle agitation. During this time, 6 x 10^8 Caco-2 cells were detached from tissue culture plates using 10 mM EDTA in PBS. Cells were split into three aliquots, cooled to 4°C, and pelleted. Each pellet was resuspended in PBS pH 6.5 and sodium metaperiodate was added to a final concentration of 1.5 mM in order to gently oxidize the cell surface. Cells were then incubated with sodium metaperiodate in the dark for 15 minutes at 4°C. Cells were washed twice with PBS pH 6.5 and split into two new aliquots. TriCEPS coupled EsxA was added to one aliquot and TriCEPS coupled transferrin was added to the other aliquot and incubated for 90 minutes at 4°C with gentle agitation. Samples were then washed, lysed via sonication, and digested with trypsin. The TriCEPS reagent:ligand:receptor complex was then affinity purified and peptides were identified using LC-MS analysis.

Immunoprecipitation

EsxA was expressed and purified as described above. EsxA or PBS alone was then biotinylated by the Sulfo-SBED reagent (Thermo 33033) according to the manufacturer instructions and excess reagent was removed using PD-10 columns (GE Healthcare 17-0851-01). 1 x 10^7 HBE cells were detached from tissue culture plates using 10 mM EDTA in PBS. Cells

were washed, resuspended in HBSS, and incubated with 1.5 μM EsxA or with PBS alone for 2 hours at 4°C with gentle agitation. Cells were then washed and exposed to UV light for 30 minutes at room temperature to allow for covalent cross-linking. Cells were lysed with RIPA buffer and lysate was incubated with streptavidin-conjugated magnetic beads (Thermo 88816). Proteins were eluted by boiling and analyzed by SDS-PAGE followed by Western blotting with rabbit anti-SR-B1 antibody (Abcam 52629).

Mouse NALT/human adenoid immunofluorescence

Mouse NALT sections were obtained as previously described (Nair et al., 2016). Briefly, mouse NALT (after decalcification) and human adenoid specimens were embedded in paraffin, sectioned (5 μm), and mounted on glass slides. Slides were deparaffinized using xylene and ethanol washes followed by heat mediated antigen-retrieval in 10 mM sodium citrate (pH 6.0). Endogenous peroxidase activity was quenched and slides were blocked in 10% donkey serum in PBS for three hours at room temperature. Slides were washed with PBS and incubated with a 1:100 dilution of mouse NKM 16-2-4 and rabbit anti-SR-B1 in 2% donkey serum in PBS overnight at 4°C. Slides were then washed with PBS and incubated with a 1:500 dilution of AlexaFluor 568 conjugated goat-anti-mouse secondary antibody (Thermo A-11004) or with HRP conjugated donkey-anti-rabbit secondary antibody (Thermo A16023) in 2% donkey serum in PBS for 1 hour at room temperature. Slides were then washed with PBS and incubated with Cy5 tyramide (Perkin Elmer SAT705A001EA) for 8 minutes. Slides were then washed with PBS, incubated with DAPI, washed with PBS, mounted in Prolong Gold antifade reagent, and imaged using an AxioImager MN microscope (Zeiss).

Mouse intranasal infection

Mtb Erdman and all mutants were grown in 7H9 and 0.05% Tween-80 until mid-log phase. Cultures were washed three times with PBS, centrifuged to remove clumps, and sonicated to yield a single-cell suspension. Bacteria were resuspended to yield a final concentration of 1 x 10^8 bacteria in 10 µL PBS. BALB/c mice obtained from The Jackson Laboratory were infected with 10 µL of the bacterial suspension intranasally. NALT from 3-5 mice were collected, homogenized, and plated on 7H11 (Difco 283810) plates supplemented with 10% OADC to enumerate the number of bacteria deposited on Day 0. Mice were sacrificed on Day 7 post-infection and cervical lymph nodes were collected, homogenized, and plated on 7H11 plates. Plates were incubated in a 37°C incubator for 3 weeks to allow for colony formation.

Adenoid culture and infection

Adenoid samples were obtained from children undergoing elective adenoidectomy for obstructive sleep apnea. Excised adenoids were immediately placed in DMEM, subsequently dissected into 3-4 pieces depending on the size of the adenoid, weighed, and mounted in a 2% agar pad such that only the mucosal surface was exposed. The adenoid pieces were then incubated overnight at 37°C in DMEM supplemented with 20% fetal bovine serum, 2 mM L-glutamine, 1% sodium pyruvate, 1% non-essential amino acids, 1 mM HEPES, 50 ug/mL kanamycin, and 50 ug/mL ampicillin to kill commensal bacteria. The following morning, liquid cultures of GFP Mtb (Kanamycin-resistant) grown to mid-log phase were washed three times with PBS and centrifuged and sonicated to remove clumps. Bacteria were then diluted to 1 x 10^7 bacteria/mL and 1 mL of inoculum was added to the adenoid and incubated at 37°C for 1 hour. Adenoids were then washed, minced into small pieces, and pushed through a 100 µm nylon cell strainer (Corning 431752). Cells were centrifuged, washed in ACK (Ammonium-Chloride-Potassium) lysis buffer (Gibco A10492-01), and then resuspended in FACS buffer (PBS + 2% FBS). Cells were stained with a 1:100

dilution of mouse anti-EpCAM Brilliant Violet 421 (Biolegend 324219), mouse PE-NKM-16-2-4 (Miltenyi 130-102-150), or rabbit anti-SR-B1 in FACS buffer, washed, and then incubated with a 1:500 dilution of AlexaFluor 488 conjugated donkey-anti-rabbit secondary antibody (Thermo R37118). Cells were washed and fixed in 4% paraformaldehyde for one hour followed by counting on an LSRII flow cytometer and analyzed using FlowJo software.

Statistical analysis

Statistical analysis was performed using GraphPad Prism. For in vitro transwell infections to determine bacterial binding or translocation, two-tailed unpaired Student's t-test was performed. For in vitro determination of antibody staining, two-tailed unpaired Student's t-test was performed. For in vivo adenoid infections or receptor expression, the paired non-parametric Wilcoxon matched pairs signed rank test was performed. For in vivo mouse infections and determination of CFU, the non-parametric Mann-Whitney U test was performed.

Ethics statement

Human adenoids were obtained from children undergoing elective adenoidectomy for sleep apnea after informed consent was obtained from parents or guardians. This study was reviewed by the University of Texas Southwestern Institutional Review Board (protocol STU 062016-087). Animal experiments were reviewed and approved by the Institutional Animal Care and Use Committee at the University of Texas Southwestern (protocol 2017-101836) and followed the eighth edition of the Guide for the Care and Use of Laboratory Animals. The University of Texas Southwestern is accredited by the American Association for Accreditation of Laboratory Animal Care (AAALAC).

Figure legends

Fig. 1 – Mtb T7SS is necessary to mediate binding and translocation across M cells

(A) Model of Mtb T7SS. **(B,C)** Control and HBE/RajiB transwells were incubated with Mtb strains at 4°C for 1 hr and binding was analyzed by confocal microscopy **(B)** with quantification of bacterial area **(C)**. Scale bar, 20 µm. **(D)** Control and HBE/RajiB transwells were incubated with Mtb strains at 4°C for 1 hr and lysed to determine binding by quantifying bacterial CFU and comparing with the initial inoculum. **(E)** Control and HBE/RajiB transwells were incubated with Mtb strains at 37°C for 1 hr and bacterial translocation was determined by quantifying bacterial CFU from the basal compartment and comparing with the inoculum. **(F)** TEER measurements from transwells from **(E)**. **(G)** Caco-2/Raji B transwells were infected as described in **E**. Experiments shown are representative of at least 3 independent experiments. **p<0.01, ***p<0.001 as determined by Student's t-test.

Fig. 2 – Mtb EsxA is sufficient to mediate binding and translocation across M cells

(A) Control and HBE/RajiB transwells were incubated with fluorescent beads coated with EsxA, EsxB, or glycine. Translocation was determined by comparing the number of beads in the basal compartment with the inoculum. **(B)** TEER measurements from transwells from **(A)**. **(C)** Caco-2/Raji B transwells were treated as described in **A**. **(D)** Control and HBE/RajiB transwells were incubated with biotinylated EsxA and stained with NKM 16-2-4 (red) and Alexa Fluor 488 conjugated streptavidin (green). Scale bar, 30 µm. **(E-G)** Quantification of nuclei (**E**), NKM 16-2-4$^+$ cells (**F**), and EsxA$^+$ (**G**) cells from the transwells described in **(D)**. **(H)** Quantification of NKM 16-2-4 staining on EsxA$^+$ cells from the HBE/Raji B transwells described in **(D)**. Experiments shown are representative of at least 3 independent experiments. *p<0.05, **p<0.01, ***p<0.001 as determined by Student's t-test.

Fig. 3 – SR-B1 is the M cell EsxA receptor

(A) Volcano plot displaying peptides enriched when Caco-2 cells were treated either with transferrin (blue dots on left) or EsxA (red dots on right). **(B)** Western blot using an anti-SR-B1 antibody of proteins enriched after HBE cells were incubated with biotinylated EsxA or control. **(C)** Control and HBE/RajiB transwells were stained with NKM 16-2-4 and an anti-SR-B1 antibody and analyzed by confocal microscopy. Arrows denote examples of double positive cells. Scale bar, 40 μm. **(D,E)** Quantification of the number of nuclei (**D**) or SR-B1$^+$ cells (**E**) from the transwells described in **(C)**. **(F)** Quantification of NKM 16-2-4 staining on SR-B1$^+$ cells from the HBE/Raji B transwells described in **(C)**. Experiments shown are representative of at least 3 independent experiments. ***$p<0.001$ as determined by Student's t-test.

Fig. 4 – Loss of SR-B1 reduces EsxA binding and Mtb translocation through M cells

(A) Western blot of SR-B1 (top) or beta-actin (bottom) of shRNA expressing HBE cells. **(B)** HBE/RajiB transwells with shRNA expressing HBE cells were incubated with biotinylated EsxA and stained with NKM 16-2-4 (red), anti-SR-B1 (cyan), and Alexa Fluor 488 conjugated streptavidin (green). Arrows denote examples of triple positive cells. Scale bar, 40 μm. **(C-E)** Quantification of the number of NKM$^+$ (**C**), SR-B1$^+$ cells (**D**) and EsxA$^+$ cells (**E**) on transwells described from **(B)**. **(F)** Quantification of SR-B1 staining on EsxA$^+$ cells from HBE NT shRNA/Raji B transwells described in **(B)**. **(G,H)** HBE/RajiB transwells with shRNA expressing HBE cells were incubated with mCherry Mtb and Mtb binding was analyzed by confocal microscopy (**G**) with quantification of bacterial staining (**H**). Scale bar, 10 μm. **(I)** HBE/RajiB transwells with shRNA expressing HBE cells were incubated with Mtb strains at 4°C and lysed to

523 determine binding by quantifying bacterial CFU and comparing with the initial inoculum. **(J)**
524 HBE/RajiB transwells with shRNA expressing HBE cells were incubated with Mtb strains at 37°C
525 and bacterial translocation was determined by quantifying bacterial CFU from the basal
526 compartment and comparing with the inoculum. **(K)** TEER of the transwells from **(J)**. (**L**)
527 HBE/RajiB transwells with shRNA expressing HBE cells were incubated with *Pseudomonas*
528 *aeruginosa* at 37°C and bacterial translocation was determined by quantifying bacterial CFU from
529 the basal compartment and comparing with the inoculum. Experiments shown are representative
530 of at least 3 independent experiments. **p<0.01, ***p<0.001 as determined by Student's t-test.
531
532 **Fig. 5 –The Mtb type VII secretion system is necessary for Mtb translocation in mice and**
533 **humans**
534 **(A)** Mouse NALT sections were stained with NKM 16-2-4 and anti-SR-B1 antibodies and
535 analyzed by confocal microscopy. Scale bar, top, 15 µm, bottom, 5 µm. **(B,C)** Mice were
536 intranasally infected with either WT Mtb, MtbΔeccD1 (**B**), or MtbΔesxA (**C**). CFU was
537 determined in the NALT on day 0 (left) or in the cervical lymph nodes on day 7 (right). Symbols
538 represent CFU from individual animals (n=8-10 per strain). ***p<0.001 compared to WT by
539 Mann-Whitney U test. **(D)** Human adenoid sections were stained with NKM 16-2-4 and anti-SR-
540 B1 antibodies and analyzed by confocal microscopy. Scale bar, top, 15 µm, bottom, 5 µm. **(E)**
541 Human adenoids were disaggregated, stained with NKM 16-2-4 and anti-EpCAM antibodies, and
542 analyzed by flow cytometry. **(F)** Human adenoids were treated as in (**E**), stained with anti-SR-B1
543 or control IgG antibodies and analyzed by flow cytometry. Symbols represent adenoids from
544 individual donor (**F-H**). **p<0.01, Wilcoxon matched pairs signed rank test. **(G)** Human adenoids
545 were infected with GFP^+ Mtb, disaggregated, immunostained and analyzed by flow cytometry to

546 determine the proportion of GFP$^+$ Mtb containing NKM$^+$/EpCAM$^+$ and NKM$^-$/EpCAM$^+$ cells.
547 *p<0.05, Wilcoxon matched pairs signed rank test. **(H)** Human adenoids were infected with GFP$^+$
548 Mtb or GFP$^+$ MtbΔ*eccD1*. The percentage of GFP$^+$ Mtb containing NKM$^+$/EpCAM$^+$ double
549 positive cells was determined by flow cytometry. The Wilcoxon matched pairs signed rank test
550 was used for comparison.
551
552 **Supplemental Fig. 1 – Recombinant EsxA and SR-B1 colocalize with the M cell marker Sialyl**
553 **Lewis^A on Raji B treated transwells**
554 **(A)** HBE/Raji B or control transwells were incubated with biotinylated EsxA and stained with anti-
555 Sialyl Lewis^A (red), anti-SR-B1 (cyan), and Alexa Fluor 488 conjugated streptavidin (green). Scale
556 bar, 30 μm. **(B-E)** Multiple images of the transwells described in (**A**) were taken and the number
557 of nuclei (**B**), SLA$^+$ (**C**), EsxA$^+$ (**D**), and SR-B1$^+$ (**E**) cells was determined using ImageJ. **(F-H)**
558 Expression of SLA on EsxA$^+$ cells (**F**), of SR-B1 on EsxA$^+$ cells (**G**), and the expression of SLA
559 on SR-B1$^+$ cells (**H**) on HBE/Raji B transwells was determined by ImageJ.
560 *p<0.05,**p<0.01,***p<0.001 as determined by Student's t-test.
561
562 **Supplemental Fig. 2 – Mtbcor::Tn7 does not display a translocation defect following a mouse**
563 **intranasal infection**
564 Mice were intranasally infected with either WT Mtb or Mtbcor::Tn7. CFU was determined in the
565 NALT on day 0 (left) or in the cervical lymph nodes on day 7 (right). Symbols represent CFU
566 from individual animals (n=8 per strain).
567
568 **Supplemental Fig. 3 – Adenoid gating strategy to determine SR-B1 positive cells**

(A-C) Gating strategy for unstained cells. Debris was excluded using FSC-A and SSC-A to yield the live cell population (**A**). Single cells were identified using the FSC-A and FSC-W (**B**) and singlets were identified using SSC-A and SSC-W (**C**). Gates for stained samples were established using unstained samples. **(D-F)** Adenoids were stained with mouse BV421 conjugated anti-EpCAM, mouse PE conjugated NKM 16-2-4, and a rabbit IgG followed by a donkey-anti-rabbit 488 conjugated antibody. Using the gating strategy described in (**A-C**), $NKM^+/EpCAM^+$ cells (highlighted in red) and $NKM^-/EpCAM^+$ cells (highlighted in blue) were analyzed for fluorescence in the green channel. **(G-I)** Adenoids were stained with mouse BV421 conjugated anti-EpCAM, mouse PE conjugated NKM 16-2-4, and rabbit anti-SR-B1 followed by a donkey-anti-rabbit 488 conjugated antibody. Using the gating strategy described in (**A-C**), $NKM^+/EpCAM^+$ cells (highlighted in red) and $NKM^-/EpCAM^+$ cells (highlighted in blue) were analyzed for fluorescence in the green channel.

Supplemental Fig. 4 – Adenoid gating strategy to determine GFP+ Mtb containing cells

(A-C) Gating strategy for unstained cells. Debris was excluded using FSC-A and SSC-A to yield the live cell population (**A**). Single cells were identified using the FSC-A and FSC-W (**B**) and singlets were identified using SSC-A and SSC-W (**C**). Gates for stained samples were established using unstained samples. **(D-F)** Adenoids were infected with a vehicle control, disaggregated, and stained with mouse BV421 conjugated anti-EpCAM and mouse PE conjugated NKM 16-2-4. Using the gating strategy described in (**A-C**), $NKM^+/EpCAM^+$ cells (highlighted in red) and $NKM^-/EpCAM^+$ cells (highlighted in blue) were analyzed for fluorescence in the green channel. **(G-I)** Adenoids were infected with GFP Mtb, disaggregated, and stained with mouse BV421 conjugated anti-EpCAM and mouse PE conjugated NKM 16-2-4. Using the gating strategy described in (**A-**

592 **C**), $NKM^+/EpCAM^+$ cells (highlighted in red) and $NKM^-/EpCAM^+$ cells (highlighted in blue) were
593 analyzed for fluorescence in the green channel.
594
595 **References:**

596 Abdallah, A.M., N.C. Gey van Pittius, P.A. Champion, J. Cox, J. Luirink, C.M. Vandenbroucke-
597 Grauls, B.J. Appelmelk, and W. Bitter. 2007. Type VII secretion--mycobacteria show the way.
598 *Nat Rev Microbiol* 5:883-891.
599 Augenstreich, J., A. Arbues, R. Simeone, E. Haanappel, A. Wegener, F. Sayes, F. Le Chevalier,
600 C. Chalut, W. Malaga, C. Guilhot, R. Brosch, and C. Astarie-Dequeker. 2017. ESX-1 and
601 phthiocerol dimycocerosates of Mycobacterium tuberculosis act in concert to cause
602 phagosomal rupture and host cell apoptosis. *Cell Microbiol* 19:
603 Behr, M.A., M.A. Wilson, W.P. Gill, H. Salamon, G.K. Schoolnik, S. Rane, and P.M. Small. 1999.
604 Comparative genomics of BCG vaccines by whole-genome DNA microarray. *Science*
605 284:1520-1523.
606 Bocharov, A.V., I.N. Baranova, T.G. Vishnyakova, A.T. Remaley, G. Csako, F. Thomas, A.P.
607 Patterson, and T.L. Eggerman. 2004. Targeting of scavenger receptor class B type I by
608 synthetic amphipathic alpha-helical-containing peptides blocks lipopolysaccharide (LPS)
609 uptake and LPS-induced pro-inflammatory cytokine responses in THP-1 monocyte cells. *J*
610 *Biol Chem* 279:36072-36082.
611 Brandtzaeg, P., H. Kiyono, R. Pabst, and M.W. Russell. 2008. Terminology: nomenclature of
612 mucosa-associated lymphoid tissue. *Mucosal Immunol* 1:31-37.

613 Churchyard, G., P. Kim, N.S. Shah, R. Rustomjee, N. Gandhi, B. Mathema, D. Dowdy, A. Kasmar,
614 and V. Cardenas. 2017. What We Know About Tuberculosis Transmission: An Overview. *J*
615 *Infect Dis* 216:S629-S635.
616 Cohen, S.B., B.H. Gern, J.L. Delahaye, K.N. Adams, C.R. Plumlee, J.K. Winkler, D.R. Sherman,
617 M.Y. Gerner, and K.B. Urdahl. 2018. Alveolar Macrophages Provide an Early Mycobacterium
618 tuberculosis Niche and Initiate Dissemination. *Cell Host Microbe* 24:439-446 e434.
619 Conrad, W.H., M.M. Osman, J.K. Shanahan, F. Chu, K.K. Takaki, J. Cameron, D. Hopkinson-
620 Woolley, R. Brosch, and L. Ramakrishnan. 2017. Mycobacterial ESX-1 secretion system
621 mediates host cell lysis through bacterium contact-dependent gross membrane disruptions.
622 *Proc Natl Acad Sci U S A* 114:1371-1376.
623 Corr, S.C., C.C. Gahan, and C. Hill. 2008. M-cells: origin, morphology and role in mucosal
624 immunity and microbial pathogenesis. *FEMS Immunol Med Microbiol* 52:2-12.
625 Cozens, A.L., M.J. Yezzi, K. Kunzelmann, T. Ohrui, L. Chin, K. Eng, W.E. Finkbeiner, J.H.
626 Widdicombe, and D.C. Gruenert. 1994. CFTR expression and chloride secretion in polarized
627 immortal human bronchial epithelial cells. *Am J Respir Cell Mol Biol* 10:38-47.
628 Feltcher, M.E., J.T. Sullivan, and M. Braunstein. 2010. Protein export systems of Mycobacterium
629 tuberculosis: novel targets for drug development? *Future Microbiol* 5:1581-1597.
630 Fontanilla, J.M., A. Barnes, and C.F. von Reyn. 2011. Current diagnosis and management of
631 peripheral tuberculous lymphadenitis. *Clin Infect Dis* 53:555-562.
632 Forbes, B., A. Shah, G.P. Martin, and A.B. Lansley. 2003. The human bronchial epithelial cell line
633 16HBE14o- as a model system of the airways for studying drug transport. *Int J Pharm*
634 257:161-167.

635 Fox, G.J., M. Orlova, and E. Schurr. 2016. Tuberculosis in Newborns: The Lessons of the "Lubeck
636 Disaster" (1929-1933). *PLoS Pathog* 12:e1005271.
637 Fujimura, Y. 2000. Evidence of M cells as portals of entry for antigens in the nasopharyngeal
638 lymphoid tissue of humans. *Virchows Arch* 436:560-566.
639 Giannasca, P.J., K.T. Giannasca, A.M. Leichtner, and M.R. Neutra. 1999. Human intestinal M
640 cells display the sialyl Lewis A antigen. *Infect Immun* 67:946-953.
641 Hase, K., K. Kawano, T. Nochi, G.S. Pontes, S. Fukuda, M. Ebisawa, K. Kadokura, T. Tobe, Y.
642 Fujimura, S. Kawano, A. Yabashi, S. Waguri, G. Nakato, S. Kimura, T. Murakami, M. Iimura,
643 K. Hamura, S. Fukuoka, A.W. Lowe, K. Itoh, H. Kiyono, and H. Ohno. 2009. Uptake through
644 glycoprotein 2 of FimH(+) bacteria by M cells initiates mucosal immune response. *Nature*
645 462:226-230.
646 Heo, T.H., S.M. Lee, B. Bartosch, F.L. Cosset, and C.Y. Kang. 2006. Hepatitis C virus E2 links
647 soluble human CD81 and SR-B1 protein. *Virus Res* 121:58-64.
648 Huang, L., K.L. Chambliss, X. Gao, I.S. Yuhanna, E. Behling-Kelly, S. Bergaya, M. Ahmed, P.
649 Michaely, K. Luby-Phelps, A. Darehshouri, L. Xu, E.A. Fisher, W.P. Ge, C. Mineo, and P.W.
650 Shaul. 2019. SR-B1 drives endothelial cell LDL transcytosis via DOCK4 to promote
651 atherosclerosis. *Nature* 569:565-569.
652 Huang, Y., and R.W. Mahley. 2014. Apolipoprotein E: structure and function in lipid metabolism,
653 neurobiology, and Alzheimer's diseases. *Neurobiol Dis* 72 Pt A:3-12.
654 Kerneis, S., A. Bogdanova, J.P. Kraehenbuhl, and E. Pringault. 1997. Conversion by Peyer's patch
655 lymphocytes of human enterocytes into M cells that transport bacteria. *Science* 277:949-952.
656 Kim, D.Y., A. Sato, S. Fukuyama, H. Sagara, T. Nagatake, I.G. Kong, K. Goda, T. Nochi, J.
657 Kunisawa, S. Sato, Y. Yokota, C.H. Lee, and H. Kiyono. 2011. The airway antigen sampling

system: respiratory M cells as an alternative gateway for inhaled antigens. *J Immunol* 186:4253-4262.

Kimura, S. 2018. Molecular insights into the mechanisms of M-cell differentiation and transcytosis in the mucosa-associated lymphoid tissues. *Anat Sci Int* 93:23-34.

Kimura, S., M. Mutoh, M. Hisamoto, H. Saito, S. Takahashi, T. Asakura, M. Ishii, Y. Nakamura, J. Iida, K. Hase, and T. Iwanaga. 2019. Airway M Cells Arise in the Lower Airway Due to RANKL Signaling and Reside in the Bronchiolar Epithelium Associated With iBALT in Murine Models of Respiratory Disease. *Front Immunol* 10:1323.

Kinhikar, A.G., I. Verma, D. Chandra, K.K. Singh, K. Weldingh, P. Andersen, T. Hsu, W.R. Jacobs, Jr., and S. Laal. 2010. Potential role for ESAT6 in dissemination of M. tuberculosis via human lung epithelial cells. *Mol Microbiol* 75:92-106.

Mabbott, N.A., D.S. Donaldson, H. Ohno, I.R. Williams, and A. Mahajan. 2013. Microfold (M) cells: important immunosurveillance posts in the intestinal epithelium. *Mucosal Immunol* 6:666-677.

Manzoni, G., C. Marinach, S. Topcu, S. Briquet, M. Grand, M. Tolle, M. Gransagne, J. Lescar, C. Andolina, J.F. Franetich, M.B. Zeisel, T. Huby, E. Rubinstein, G. Snounou, D. Mazier, F. Nosten, T.F. Baumert, and O. Silvie. 2017. Plasmodium P36 determines host cell receptor usage during sporozoite invasion. *Elife* 6:

Mutoh, M., S. Kimura, H. Takahashi-Iwanaga, M. Hisamoto, T. Iwanaga, and J. Iida. 2016. RANKL regulates differentiation of microfold cells in mouse nasopharynx-associated lymphoid tissue (NALT). *Cell Tissue Res* 364:175-184.

679 Nair, V.R., L.H. Franco, V.M. Zacharia, H.S. Khan, C.E. Stamm, W. You, D.K. Marciano, H.
680 Yagita, B. Levine, and M.U. Shiloh. 2016. Microfold Cells Actively Translocate
681 Mycobacterium tuberculosis to Initiate Infection. *Cell Rep* 16:1253-1258.
682 Nakamura, Y., S. Kimura, and K. Hase. 2018. M cell-dependent antigen uptake on follicle-
683 associated epithelium for mucosal immune surveillance. *Inflamm Regen* 38:15.
684 Nakato, G., K. Hase, M. Suzuki, M. Kimura, M. Ato, M. Hanazato, M. Tobiume, M. Horiuchi, R.
685 Atarashi, N. Nishida, M. Watarai, K. Imaoka, and H. Ohno. 2012. Cutting Edge: Brucella
686 abortus exploits a cellular prion protein on intestinal M cells as an invasive receptor. *J*
687 *Immunol* 189:1540-1544.
688 Nochi, T., Y. Yuki, A. Matsumura, M. Mejima, K. Terahara, D.Y. Kim, S. Fukuyama, K. Iwatsuki-
689 Horimoto, Y. Kawaoka, T. Kohda, S. Kozaki, O. Igarashi, and H. Kiyono. 2007. A novel M
690 cell-specific carbohydrate-targeted mucosal vaccine effectively induces antigen-specific
691 immune responses. *J Exp Med* 204:2789-2796.
692 Park, H.S., K.P. Francis, J. Yu, and P.P. Cleary. 2003. Membranous cells in nasal-associated
693 lymphoid tissue: a portal of entry for the respiratory mucosal pathogen group A streptococcus.
694 *J Immunol* 171:2532-2537.
695 Pathak, S.K., S. Basu, K.K. Basu, A. Banerjee, S. Pathak, A. Bhattacharyya, T. Kaisho, M. Kundu,
696 and J. Basu. 2007. Direct extracellular interaction between the early secreted antigen ESAT-
697 6 of Mycobacterium tuberculosis and TLR2 inhibits TLR signaling in macrophages. *Nat*
698 *Immunol* 8:610-618.
699 Philips, J.A., E.J. Rubin, and N. Perrimon. 2005. Drosophila RNAi screen reveals CD36 family
700 member required for mycobacterial infection. *Science* 309:1251-1253.

Santander, N.G., S. Contreras-Duarte, M.F. Awad, C. Lizama, I. Passalacqua, A. Rigotti, and D. Busso. 2013. Developmental abnormalities in mouse embryos lacking the HDL receptor SR-BI. *Hum Mol Genet* 22:1086-1096.

Schafer, G., R. Guler, G. Murray, F. Brombacher, and G.D. Brown. 2009. The role of scavenger receptor B1 in infection with Mycobacterium tuberculosis in a murine model. *PLoS One* 4:e8448.

Shen, W.J., S. Azhar, and F.B. Kraemer. 2018. SR-B1: A Unique Multifunctional Receptor for Cholesterol Influx and Efflux. *Annu Rev Physiol* 80:95-116.

Smith, J., J. Manoranjan, M. Pan, A. Bohsali, J. Xu, J. Liu, K.L. McDonald, A. Szyk, N. LaRonde-LeBlanc, and L.Y. Gao. 2008. Evidence for pore formation in host cell membranes by ESX-1-secreted ESAT-6 and its role in Mycobacterium marinum escape from the vacuole. *Infect Immun* 76:5478-5487.

Sreejit, G., A. Ahmed, N. Parveen, V. Jha, V.L. Valluri, S. Ghosh, and S. Mukhopadhyay. 2014. The ESAT-6 protein of Mycobacterium tuberculosis interacts with beta-2-microglobulin (beta2M) affecting antigen presentation function of macrophage. *PLoS Pathog* 10:e1004446.

Srinivasan, B., A.R. Kolli, M.B. Esch, H.E. Abaci, M.L. Shuler, and J.J. Hickman. 2015. TEER measurement techniques for in vitro barrier model systems. *J Lab Autom* 20:107-126.

Stamm, C.E., A.C. Collins, and M.U. Shiloh. 2015. Sensing of Mycobacterium tuberculosis and consequences to both host and bacillus. *Immunol Rev* 264:204-219.

Stanley, S.A., S. Raghavan, W.W. Hwang, and J.S. Cox. 2003. Acute infection and macrophage subversion by Mycobacterium tuberculosis require a specialized secretion system. *Proc Natl Acad Sci U S A* 100:13001-13006.

Teitelbaum, R., W. Schubert, L. Gunther, Y. Kress, F. Macaluso, J.W. Pollard, D.N. McMurray, and B.R. Bloom. 1999. The M cell as a portal of entry to the lung for the bacterial pathogen Mycobacterium tuberculosis. *Immunity* 10:641-650.

Tremblay, T.L., and J.J. Hill. 2017. Biotin-transfer from a trifunctional crosslinker for identification of cell surface receptors of soluble protein ligands. *Sci Rep* 7:46574.

Trigatti, B., H. Rayburn, M. Vinals, A. Braun, H. Miettinen, M. Penman, M. Hertz, M. Schrenzel, L. Amigo, A. Rigotti, and M. Krieger. 1999. Influence of the high density lipoprotein receptor SR-BI on reproductive and cardiovascular pathophysiology. *Proc Natl Acad Sci U S A* 96:9322-9327.

Tschernig, T., and R. Pabst. 2000. Bronchus-associated lymphoid tissue (BALT) is not present in the normal adult lung but in different diseases. *Pathobiology* 68:1-8.

Tyrer, P., A.R. Foxwell, A.W. Cripps, M.A. Apicella, and J.M. Kyd. 2006. Microbial pattern recognition receptors mediate M-cell uptake of a gram-negative bacterium. *Infect Immun* 74:625-631.

Yang, Z., Y. Kong, F. Wilson, B. Foxman, A.H. Fowler, C.F. Marrs, M.D. Cave, and J.H. Bates. 2004. Identification of risk factors for extrapulmonary tuberculosis. *Clin Infect Dis* 38:199-205.

Zacharia, V.M., P.S. Manzanillo, V.R. Nair, D.K. Marciano, L.N. Kinch, N.V. Grishin, J.S. Cox, and M.U. Shiloh. 2013. cor, a novel carbon monoxide resistance gene, is essential for Mycobacterium tuberculosis pathogenesis. *MBio* 4:e00721-00713.

Zanoni, P., S.A. Khetarpal, D.B. Larach, W.F. Hancock-Cerutti, J.S. Millar, M. Cuchel, S. DerOhannessian, A. Kontush, P. Surendran, D. Saleheen, S. Trompet, J.W. Jukema, A. De Craen, P. Deloukas, N. Sattar, I. Ford, C. Packard, A. Majumder, D.S. Alam, E. Di

746 Angelantonio, G. Abecasis, R. Chowdhury, J. Erdmann, B.G. Nordestgaard, S.F. Nielsen, A.
747 Tybjaerg-Hansen, R.F. Schmidt, K. Kuulasmaa, D.J. Liu, M. Perola, S. Blankenberg, V.
748 Salomaa, S. Mannisto, P. Amouyel, D. Arveiler, J. Ferrieres, M. Muller-Nurasyid, M.
749 Ferrario, F. Kee, C.J. Willer, N. Samani, H. Schunkert, A.S. Butterworth, J.M. Howson, G.M.
750 Peloso, N.O. Stitziel, J. Danesh, S. Kathiresan, D.J. Rader, C.H.D.E. Consortium, C.A.E.
751 Consortium, and C. Global Lipids Genetics. 2016. Rare variant in scavenger receptor BI raises
752 HDL cholesterol and increases risk of coronary heart disease. *Science* 351:1166-1171.

753 **Acknowledgments:** We thank Beth Levine and members of the Shiloh Lab for constructive
754 feedback on the manuscript. This work is supported by the Burroughs Wellcome Fund 1017894
755 (MUS), Welch Foundation I-1964-20180324 (MUS), NIH U01 AI125939-04 (MUS), NIH U19
756 AI142784-01 (MUS) , NIH 5T32AI005284-40 (HSK), and NIH R01 HL131597-03 (PWS).

757 **Authors contributions:** Conceptualization, H.S.K, V.R.N., M.U.S.; Formal analysis, H.S.K,
758 V.R.N., M.U.S.; Funding acquisition, M.U.S.; Investigation, H.S.K., V.R.N., C.R.R., S.A.A.,
759 J.L.G.R., L.H.F.; Project administration, H.S.K., M.U.S.; Resources, L.H., P.W.S., R.M.;
760 Supervision, M.U.S.; Visualization, H.S.K.; Writing – original draft, H.S.K., M.U.S.; Writing –
761 review & editing, All authors.

762 **Competing interests:** The authors declare that they have no competing interests.

763 **Data and materials availability:** All material is available upon request. All data is available in
764 the manuscript or the supplementary materials.

Figure 1

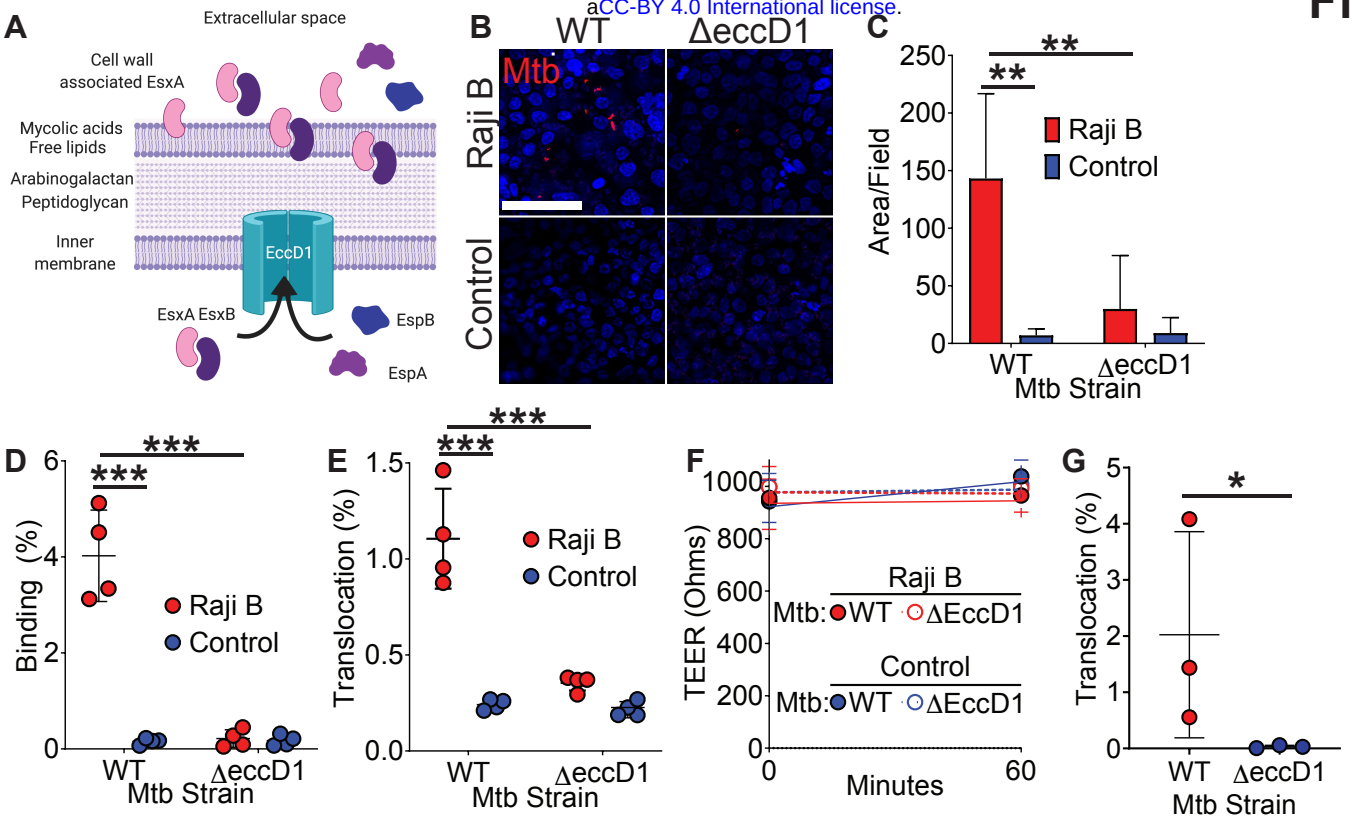

Figure 2

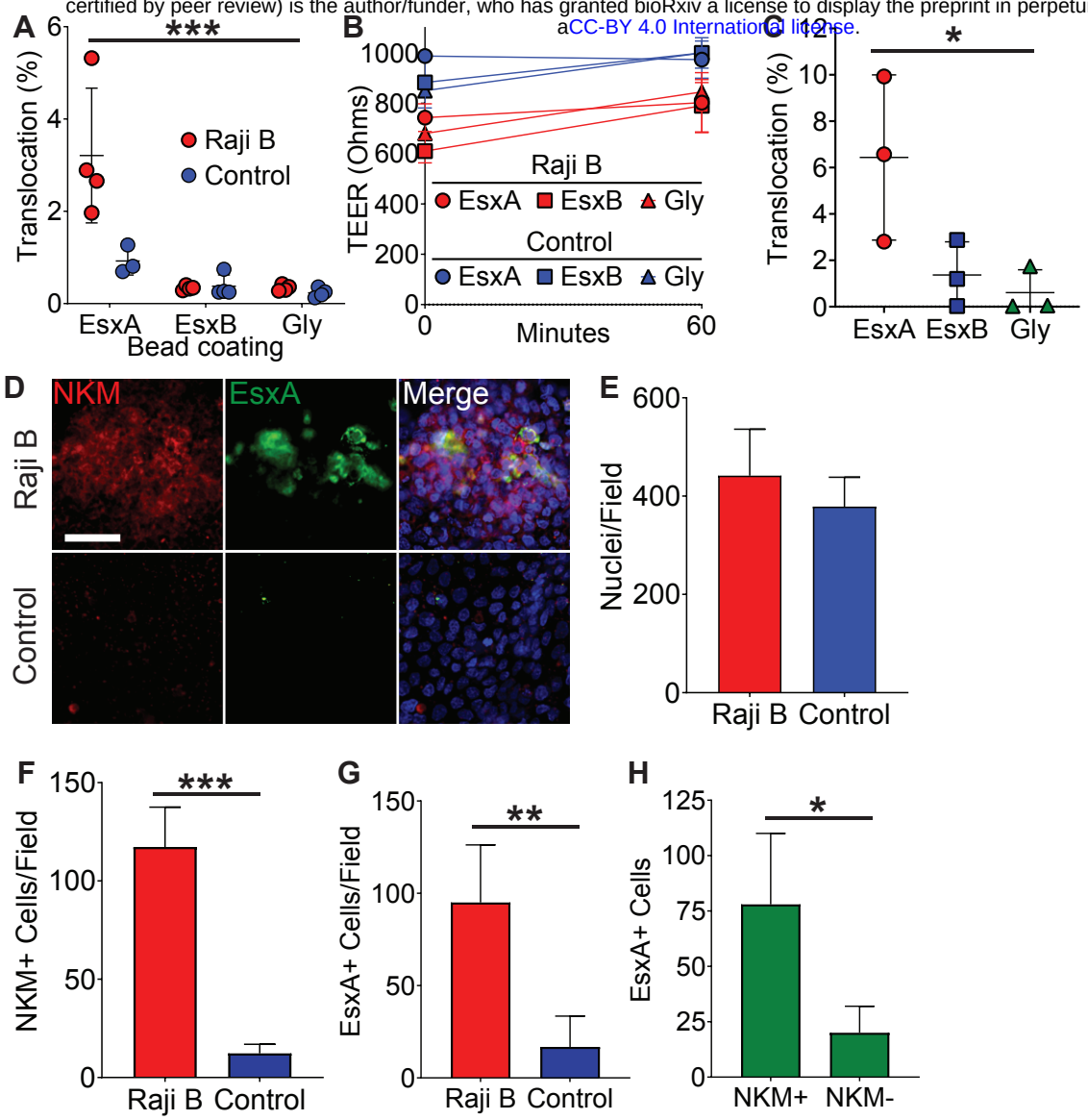

Figure 3

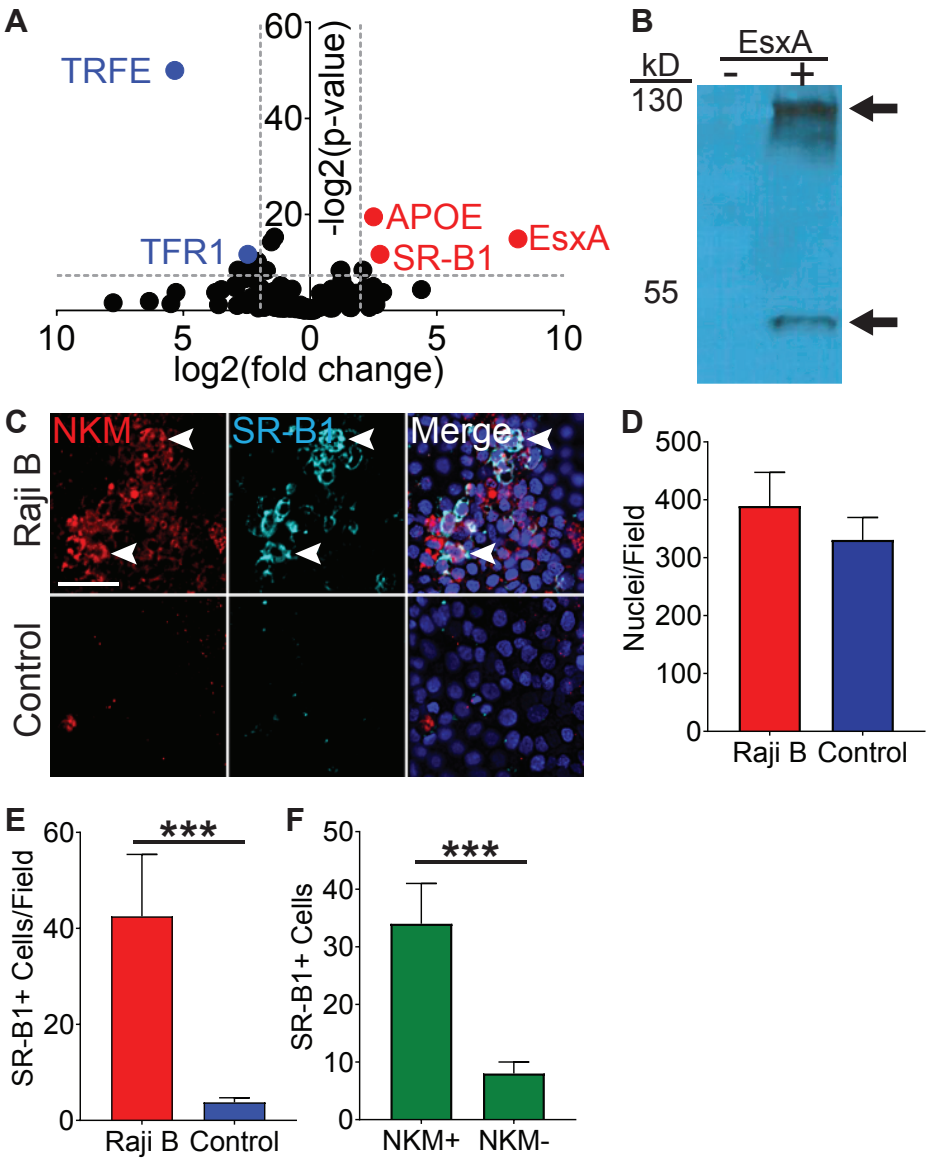

Figure 4

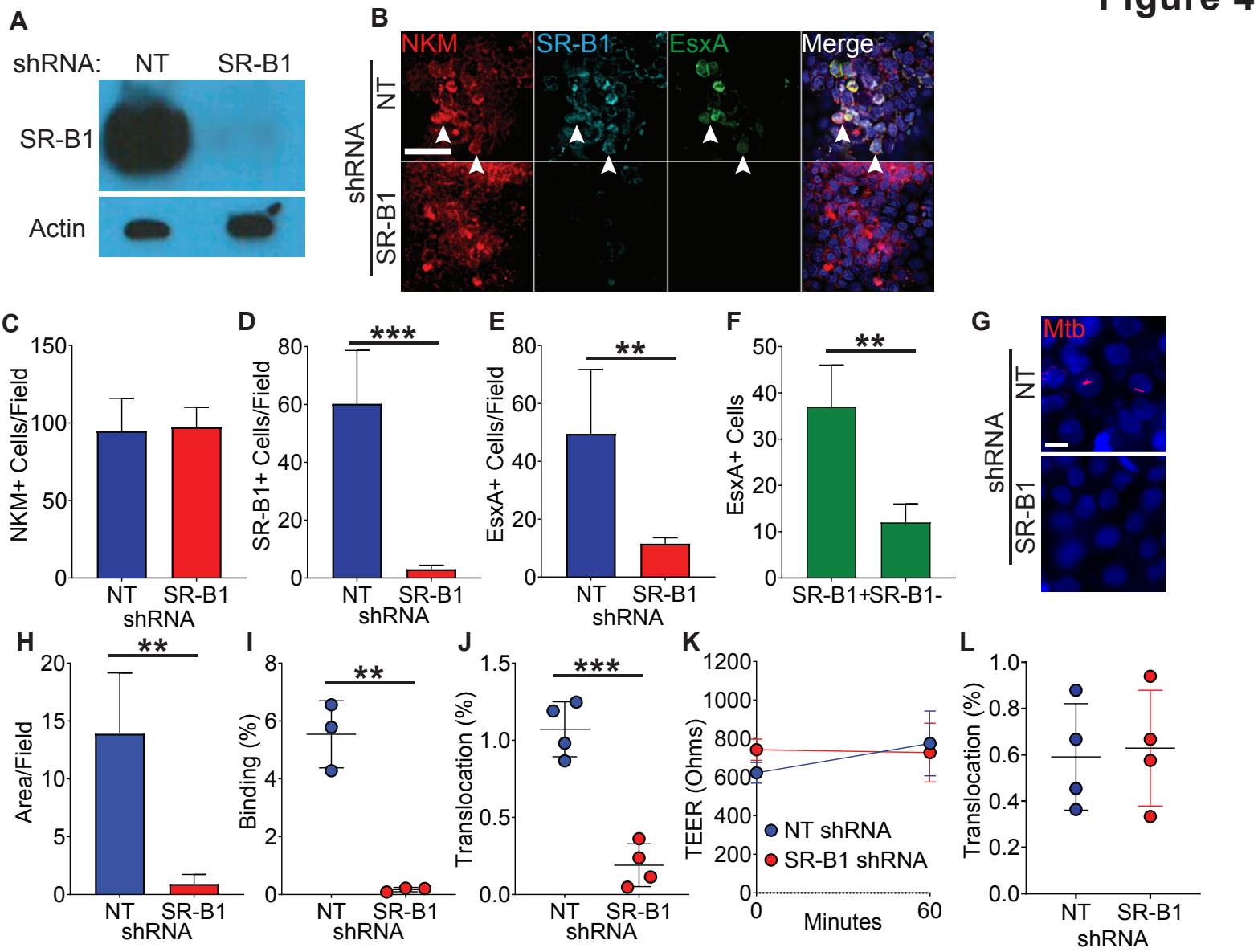

Figure 5

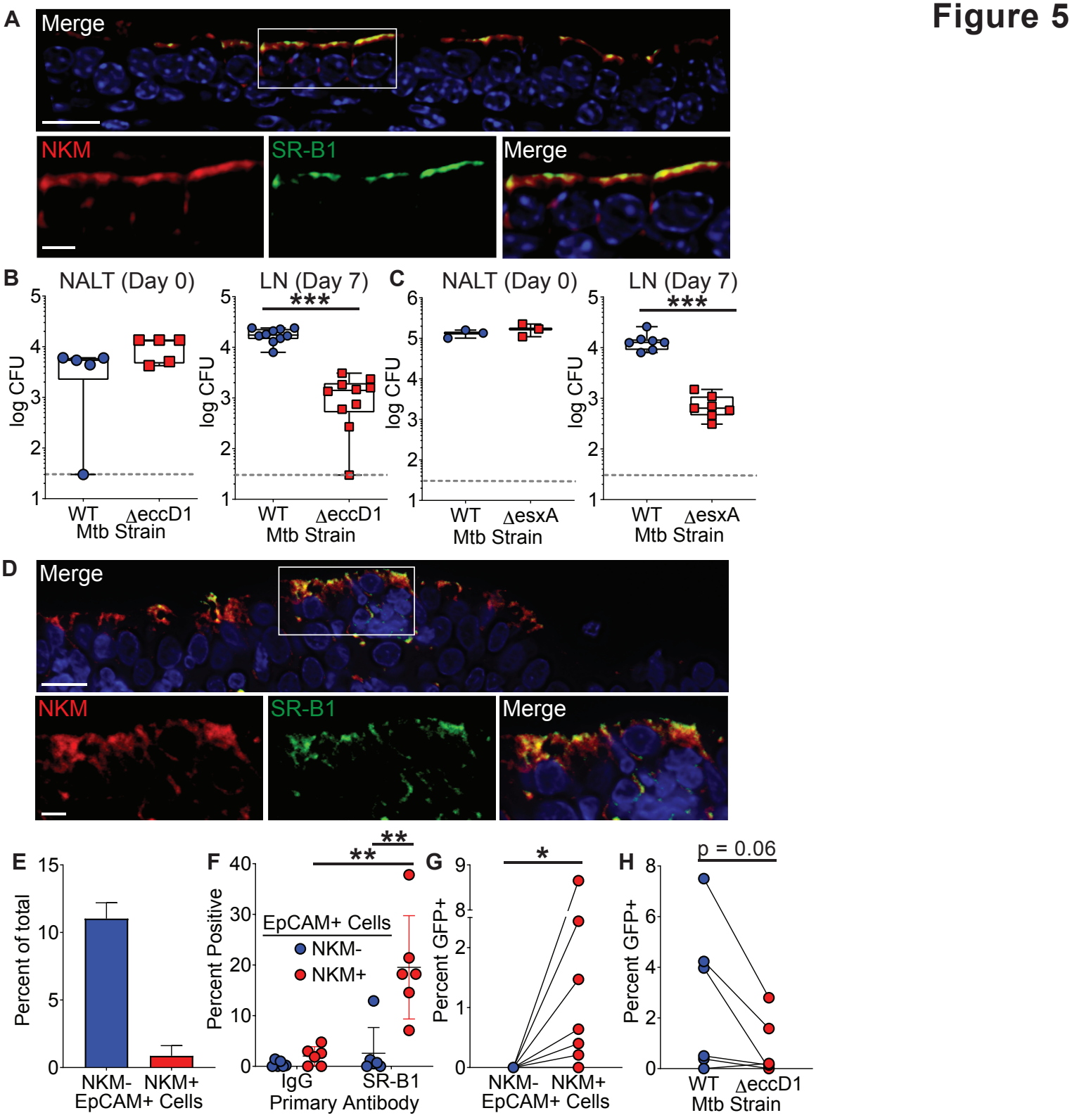

Supplemental Figure 1

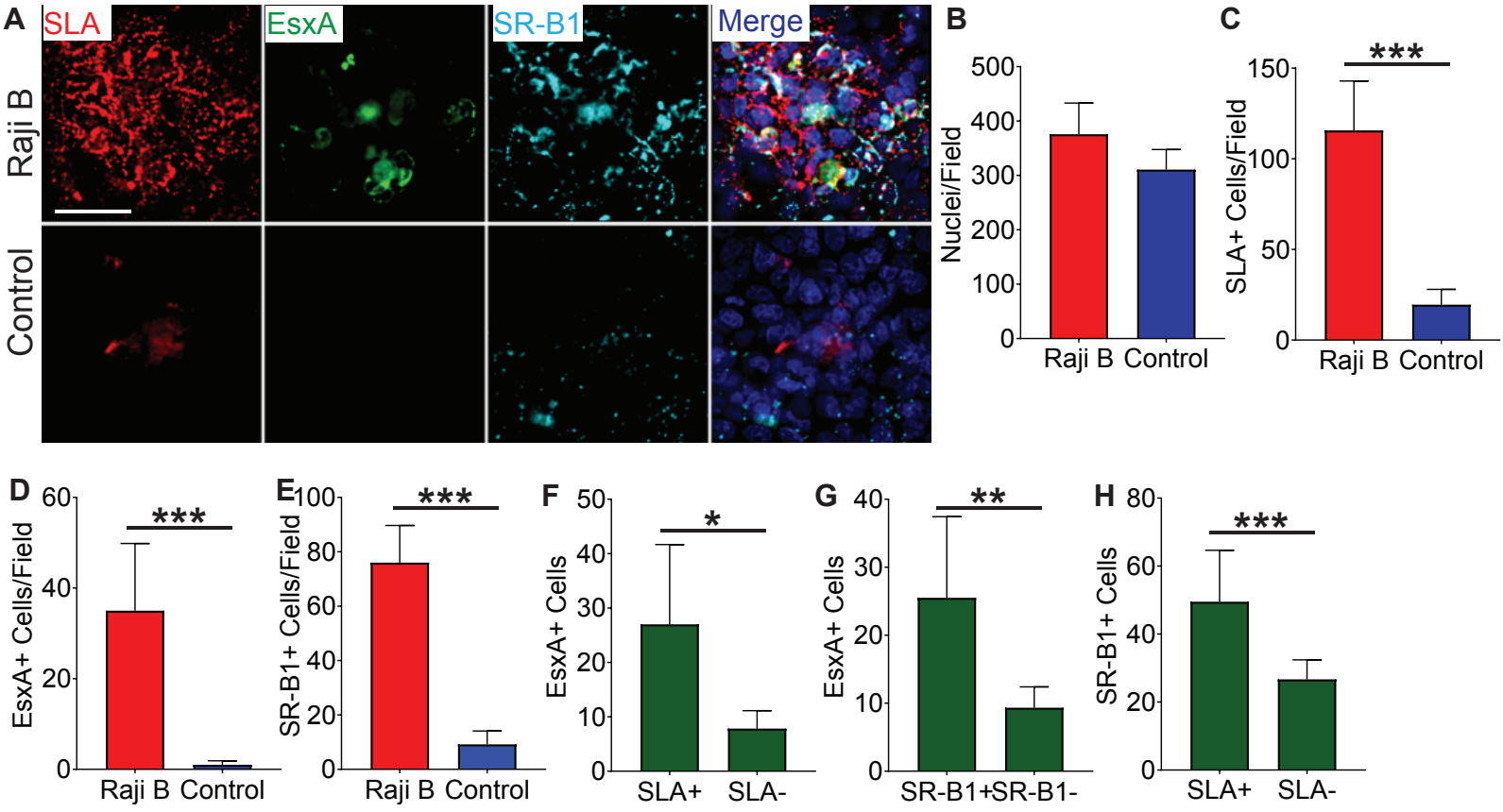

Supplemental Figure 2

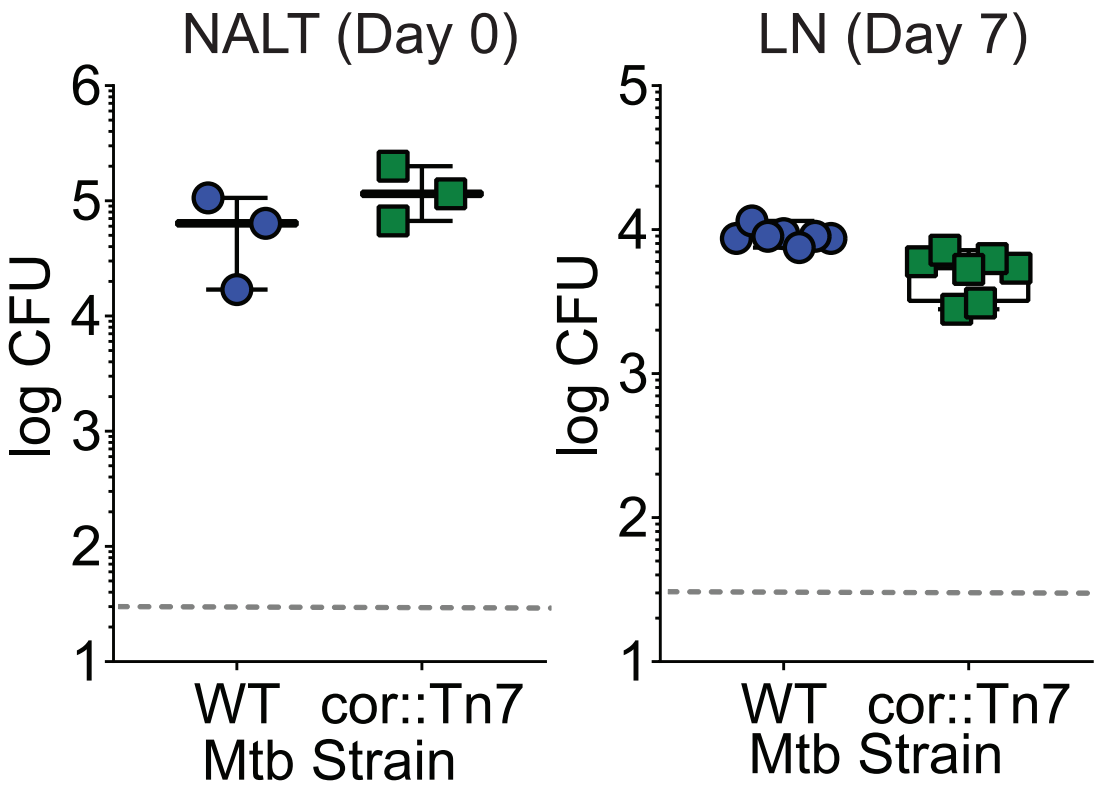

Supplemental Figure 3

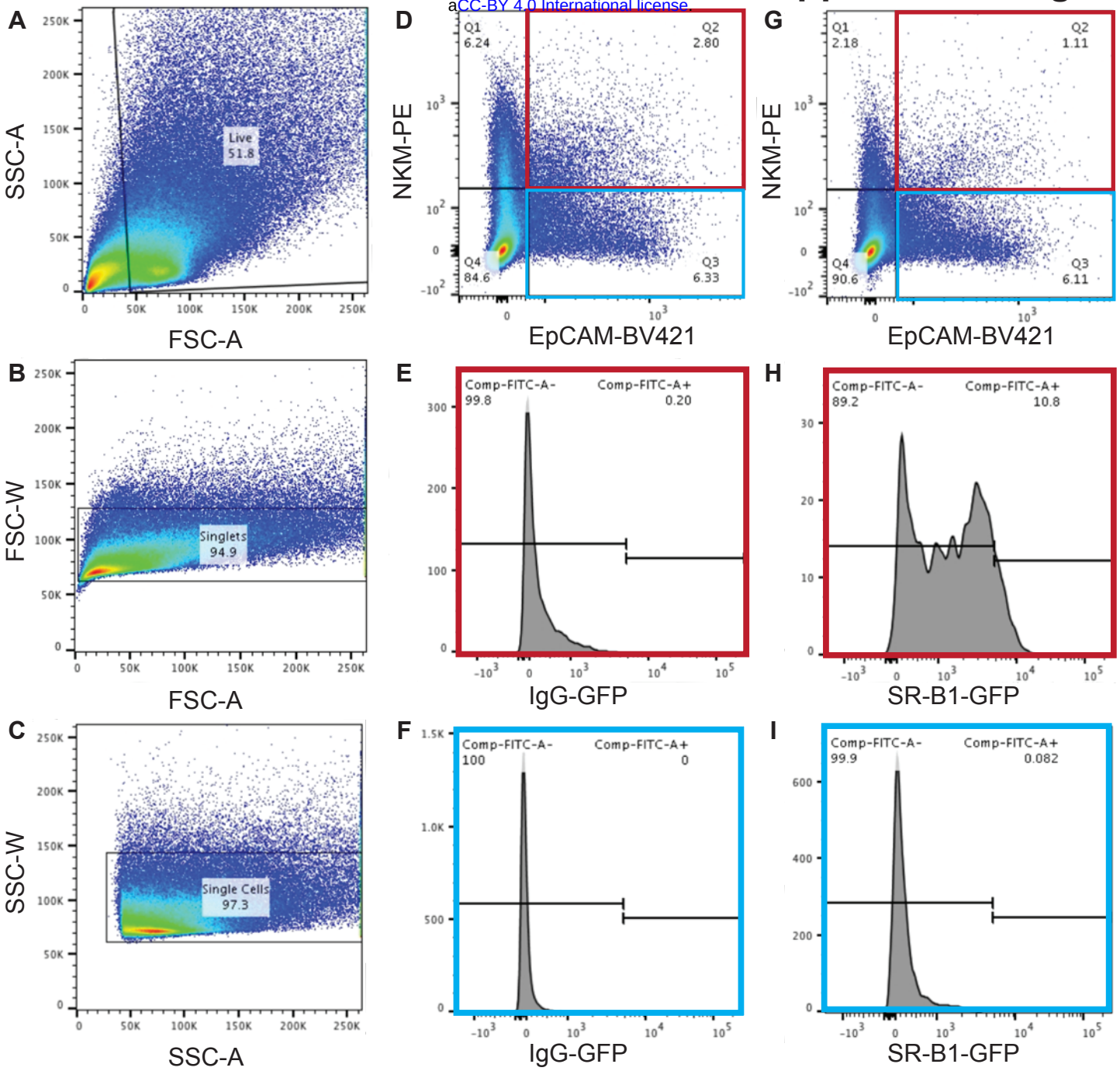

Supplemental Figure 4